Research Square

Preprints are preliminary reports that have not undergone peer review.
They should not be considered conclusive, used to inform clinical practice,
or referenced by the media as validated information.

Fibrous Rich Tumor Models Reveals Microenvironment Dependent Drug Interactions in Colorectal Cancer

Tomas Lugo
Texas Tech University
Thu Annelise Nguyen
Annelise.Nguyen@ttu.edu
Texas Tech University

Research Article

Keywords: Colorectal, Gap Junctions, 3D Models, Spheroid, Fibroblast, Drug synergy, Tumor Microenvironment, ZIP Model, Combination Therapy

Posted Date: November 2nd, 2026

DOI: https://doi.org/10.21203/rs.3.rs-10806503/v1

License: This work is licensed under a Creative Commons Attribution 4.0 International License.
Read Full License

Additional Declarations: No competing interests reported.

Abstract

Background:
Tumor response to therapy is strongly influenced by multicellular interactions within the tumor microenvironment, particularly fibroblast and tumor communication mediated by gap junctions. Traditional monoculture models fail to capture these dynamics, limiting the understanding of drug combination effects. This study evaluates the role of a gap junction enhancer (PQ) in modulating antineoplastic drug responses in three dimensional (3D) colorectal cancer models.

Methods:
3D monoculture and fibroblast coculture spheroids were generated using colorectal cancer cell lines (Caco-2, HT-29, SW480, SW620) and CCD-112CoN fibroblasts. Spheroids were treated with antineoplastic agents (Doxorubicin, Nilotinib, Cediranib, Erlotinib) alone or in combination with PQ across full dose matrices. Cell viability was measured using the RealTime-Glo assay. Drug interactions were quantified using the Zero Interaction Potency (ZIP) model, with results visualized as 2D synergy maps and 3D interaction landscapes.

Results:
PQ alone produced limited and variable effects on spheroid metabolic activity. When combined with Doxorubicin, PQ altered response profiles, with higher ZIP scores observed in Caco-2–CCD-112 co-culture spheroids than in Caco-2 monoculture spheroids. PQ–drug interactions were not uniform across dose matrices, with regions of synergy, additivity, and antagonism observed depending on drug type, concentration, and culture condition. PQ and Erlotinib in co-culture spheroids showed mostly additive to weakly antagonistic interaction patterns.

Conclusions:
PQ modified antineoplastic drug response in 3D colorectal cancer spheroid models, but its effects were dependent on drug type, dose, and culture context. These findings support the use of 3D co-culture systems and full dose–matrix analyses to evaluate context-dependent drug interactions in colorectal cancer models.

Background

Colorectal cancer (CRC) is a biologically complex and heterogeneous disease in which therapeutic response is governed not only by tumor cell intrinsic properties but also by dynamic interactions within the tumor microenvironment.[1–5] In multicellular tumor systems, stromal fibroblasts play a central role in shaping drug sensitivity and resistance through direct cell-cell contact, paracrine signaling, and metabolic coupling.[6–8] These interactions create a coordinated network that can redistribute stress signals, buffer cytotoxic damage, or promote survival pathways, fundamentally altering treatment outcomes compared to simplified monoculture systems.[9–15] As a result, conventional in vitro models often fail to capture the full spectrum of therapeutic responses observed in vivo.[15–17]

A key mediator of this intercellular coordination is gap junction intercellular communication (GJIC), which enables the direct exchange of ions, metabolites, and signaling molecules between adjacent cells.[18–23] Through connexin based GJIC channels, this communication allows tumor and stromal cells to function as a connected system rather than as isolated cells.[23,24] This connectivity has important implications for therapy, as it can facilitate the propagation of cytotoxic signals such as enhancing treatment efficacy or distribute protective signals that promote resistance.[18,19,25–28] Modulating GJIC therefore represents a potentially powerful, yet underexplored, strategy for influencing therapeutic response. However, the effects of such modulation are inherently context dependent and likely vary across drug classes, concentrations, and cellular compositions.

Importantly, drug interactions in multicellular systems are not uniform across all conditions.[29–36] The same therapeutic combination may produce synergy, additivity, or antagonism depending on the local dose environment and the state of intercellular communication. In fibroblast rich tumor systems, enhanced coupling may increase shared vulnerability at certain concentrations while promoting protective buffering at others.[37–41] This spatial and concentration dependent variability showcases the limitation of evaluating drug combinations at single concentration points and highlights the need for full dose response matrix analyses to accurately characterize interaction.

Adding another layer of complexity, CRC progression itself drives profound changes in therapeutic sensitivity.[29,42–44] As tumors evolve from well differentiated epithelial states to invasive and metastatic phenotypes, they undergo progressive alterations in genomic stability, DNA damage response, metabolic programming, and survival signaling pathways[42,45–50]. These changes shift tumors from states of high proliferative vulnerability to conditions characterized by adaptive resistance, enhanced stress tolerance, and increased reliance on microenvironmental support.[29,30,44,45,50,51] Consequently, the efficacy of both cytotoxic and targeted therapies is highly stage dependent, and responses observed in early-stage models may not translate to advanced disease.

Despite these known complexities, preclinical drug evaluation frequently relies on two dimensional (2D) monoculture systems that lack structural organization, intercellular communication, and microenvironmental context.[14,16,17,52] These models often overestimate therapeutic efficacy and fail to capture resistance mechanisms that emerge in more physiologically relevant systems.[17] Three dimensional (3D) spheroid models address these limitations by recapitulating key features of tumor biology, including cell-cell contact, diffusion gradients, and spatial heterogeneity.[14–17] When combined with fibroblast coculture, these systems more accurately reflect the tumor microenvironment and enable investigation of stromal contributions to drug response.

In parallel with advances in experimental models, analytical approaches for evaluating drug interactions have evolved. Traditional frameworks such as Highest Single Agent (HSA), Loewe additivity, and Bliss independence provide useful but limited perspectives, particularly in systems where interactions vary across concentration space.[53–56] The Zero Interaction Potency (ZIP) model offers a more

comprehensive approach by assessing deviations in potency across entire dose response surfaces, making it well suited for analyzing heterogeneous interaction patterns in complex 3D systems.[57] This is particularly relevant for agents that indirectly influence cellular behavior, such as gap junction modulators, where effects may manifest as shifts in response dynamics rather than direct cytotoxicity.

Taken together, these considerations illustrate a critical gap in current preclinical research. The lack of integrated models that simultaneously account for tumor progression, microenvironmental interactions, and dose dependent drug synergy landscapes. To address this, the present study employs 3D monoculture and fibroblast coculture spheroid systems representing multiple stages of CRC progression to investigate how modulation of gap junction communication influences therapeutic response. By combining full dose matrix experimental design with ZIP based interaction analysis, this work aims to define the context dependent role of intercellular communication in shaping drug efficacy and to identify conditions under which gap junction modulation enhances or suppresses treatment outcomes.

Methods

Study Aim, Design, and Setting

This study aimed to determine how modulation of GJIC influences antineoplastic drug response and drug interactions in CRC. A controlled vitro experimental design was employed using 3D mono-culture and fibroblast co-culture spheroid systems to model tumor microenvironment interactions across a full dose response matrix. All experiments were conducted under standardized laboratory conditions using established CRC cell lines.

Cell Lines and Materials

Human colorectal cancer cell lines (Caco-2, HT-29, SW480, and SW620) and CCD-112CoN fibroblasts were obtained from the American Type Culture Collection (ATCC, Manassas, VA, USA). Cells were cultured in Roswell Park Memorial Institute (RPMI) 1640 medium (Gibco, Thermo Fisher Scientific, Waltham, MA, USA) supplemented with 10% fetal bovine serum and 1% antibiotic and antimycotic solution.

Antineoplastic agents included Doxorubicin, Erlotinib, Nilotinib, and Cediranib. A quinolone based compound (PQ;6-methoxy-8-[(2-furanylmethyl) amino]-4-methyl-5-(3-trifluoromethylphenyloxy quinolone) was used as a GJIC enhancer.[23,58–60] All compounds were prepared according to manufacturer recommendations and diluted in culture medium immediately prior to use. Vehicle controls (0.1% dimethyl sulfoxide [DMSO]) were included in all experiments.

3D Spheroid Generation and Co-Culture System

Three-dimensional spheroids were generated using the CelVivo 3D Cell Culture System. Mono-culture spheroids were formed by seeding 20,000 tumor cells per reactor. Co-culture spheroids were generated by combining tumor cells with CCD-112CoN fibroblasts at a 1:1 ratio (10,000 cells each). Spheroids were cultured under continuous rotation, beginning at 16 rpm and increasing incrementally to support aggregation and maturation. After a two week growth period, spheroids were size-selected (150–200 µm) using sequential filtration and transferred into 96-well plates at one spheroid per well for downstream experiments.

Experimental Interventions

Experimental Interventions
Single agent treatments were conducted using a standardized concentration gradient to capture the full range of drug responses. Each antineoplastic agent (Doxorubicin, Erlotinib, Nilotinib, and Cediranib) was tested across the following concentrations: 0, 10 nM, 50 nM, 100 nM, 500 nM, 1 µM, and 10 µM. This range was selected to encompass subtherapeutic, intermediate, and high dose exposures, enabling characterization of dose dependent effects on spheroid viability.

For combination studies, GJIC enhancer PQ was applied across a concentration series of 0, 10 µM, 50 µM, 100 µM, and 200 µM. PQ concentrations were systematically combined with each concentration of the antineoplastic agents to generate dose response matrices.

Immunofluorescence and Protein Analysis

Immunofluorescence staining was performed to evaluate connexin expression and to confirm the cellular composition and structural organization of spheroids. Spheroids were gently washed with phosphate buffered saline (PBS) and fixed in 4% paraformaldehyde for 90 minutes at room temperature to preserve cellular architecture. Following fixation, samples were permeabilized using 0.25% Triton X-100 in PBS for 40 minutes to facilitate antibody penetration throughout the spheroid structure. To minimize nonspecific binding, samples were incubated in blocking buffer for 2 hours at room temperature. Spheroids were then incubated overnight at 4°C with primary antibodies diluted 1:1000 in blocking buffer. Primary antibodies targeted connexin proteins to assess gap junction expression, as well as cell type specific markers including epithelial cell adhesion molecule (EpCAM) for epithelial tumor cells and decorin (DCN) for fibroblast identification. After primary antibody incubation, samples were washed thoroughly with PBS and incubated with species appropriate Alexa Fluorconjugated secondary antibodies diluted 1:5000 in blocking buffer for 2 hours at room temperature. Following secondary incubation, spheroids were washed three times with PBS. Nuclei were counterstained with 4',6-diamidino-2-phenylindole (DAPI; 1:1000 dilution) for 10 minutes. After a final wash, spheroids were maintained in PBS and imaged directly in 96-well plates using confocal laser scanning microscopy.

Statistical and Interaction Analysis

All experiments were performed using six technical replicates per condition in each of three independent biological experiments. Technical replicates were averaged within each biological experiment before statistical summaries were calculated, unless otherwise indicated, data are presented as the mean ± standard error of the mean (SEM) from three independent biological replicates. RealTime Glo luminescence values were normalized to the corresponding time matched DMSO control for each model and biological replicate.

For time course analyses, the area under the curve (AUC) from 1 to 42 hours was calculated separately for each biological replicate. The effect of PQ on each drug response was summarized as ΔAUC, defined as AUC (drug + PQ) – AUC (drug alone). Negative ΔAUC values indicate lower time metabolic activity in the presence of PQ, whereas positive values indicate higher time integrated metabolic activity with PQ. Mean ΔAUC values and SEM were calculated across the three biological replicates.

Drug interactions between PQ and the antineoplastic agents were evaluated using the Zero Interaction Potency (ZIP) model implemented in SynergyFinder. Dose with response data were converted to percent inhibition relative to the appropriate vehicle control and analyzed as complete concentration matrices for each culture condition. ZIP δ-scores represent deviations between the observed response and the response expected under the ZIP reference model. ZIP scores greater than 10 were classified as synergistic, scores from − 10 to 10 as additive, and scores below − 10 as antagonistic. Overall ZIP scores summarize the complete dose matrix, whereas the most synergistic area score identifies the region with the strongest localized positive interaction.

All data processing, AUC calculations, statistical summaries, and figure generation were performed in R using the readxl, dplyr, tidyr, and ggplot2 packages.

Results

Connexin Expression Is Preserved Across 2D and 3D Culture Systems

Confocal imaging revealed that multiple connexin isoforms are expressed in both three-dimensional (3D) spheroid cultures and two-dimensional (2D) monolayer cells. In Caco-2 spheroids (Supplemental 1), connexin immunofluorescence was detectable for Cx43, Cx26, Cx40, with signal distributed throughout the spheroid structure. In 2D cultures (Supplemental 1), connexin expressions were similarly observed at the cellular level, with Cx26, Cx40, and Cx43 visualized in conjunction with vimentin staining. Together, these findings demonstrate that connexin expression is maintained across both 2D and 3D culture systems.

Connexin expression was further evaluated in 3D co-culture spheroids to determine whether connexin localization was maintained in a complex 3D structure. Confocal imaging of co-culture spheroids revealed detectable connexin immunofluorescence for Cx43, Cx26, and Cx32 (Supplemental 2). Across

all connexin targets, signal was observed within intact spheroid structures and was retained in merged fluorescence and brightfield images, indicating preservation of connexin expression in coculture conditions. Connexin signal frequently localized to spheroid boundaries, consistent with junctional association in a 3D environment.

Confocal imaging of Caco-2 and CCD-112 co-culture spheroids revealed clear organization of epithelial and stromal cell populations when viewed from both front and back orientations (Figs. 1). EPCAM positive Caco-2 cells formed a defined epithelial compartment enriched toward the spheroid outer core, while decorin-positive CCD-112 cells were distributed throughout the spheroid interior, consistent with stromal integration. Nuclear DAPI staining confirmed dense cellular organization across the spheroid volume. Comparable marker localization patterns observed from opposing viewing angles indicate that epithelial–stromal organization is maintained throughout the three-dimensional structure.

Confocal imaging of HT-29–CCD-112 co-culture spheroids demonstrated distinct epithelial and stromal marker when visualized from both front and back orientations (Figs. 1) EPCAM-positive HT-29 cells formed a compact epithelial population within the spheroid, while decorin-positive CCD-112 cells were interspersed throughout the surrounding structure, indicating stromal integration. DAPI nuclear staining confirmed dense cellular organization across the spheroid volume. Consistent marker distribution observed from opposing views supports the presence of stable 3D organization and sustained epithelial–stromal interactions within HT-29–CCD-112 co-culture spheroids.

Z-stack confocal imaging of SW620–CCD-112 co-culture spheroids further confirmed 3D epithelial and stromal organization within the spheroid architecture (Fig. 1). EPCAM-positive SW620 cells were observed forming a defined epithelial compartment, while decorin positive CCD-112 cells were distributed throughout the spheroid volume. The Z-stack projection demonstrated that both cell populations were maintained across multiple optical sections, indicating stable integration throughout the depth of the spheroid. Orthogonal reconstruction further demonstrated marker continuity across the z-axis and visualized the vertical cross-section plane used for analysis (Fig. 1), supporting true 3D organization of the co-culture spheroid.

Brightfield imaging was used to assess spheroid morphology under co-culture and mono-culture conditions. In Caco-2–CCD-112 co-culture spheroids (Fig. 2), spheroids appeared larger and more irregular in shape, and less sharply defined boundaries, consistent with the integration of multiple cell types within a single structure. In contrast, Caco-2 mono-culture spheroids (Fig. 2) displayed smaller, more uniform, and compact morphology with smoother edges and a more homogeneous appearance.

Confocal imaging of mono-culture spheroids expression patterns (Fig. 2). In Caco-2 mono-culture spheroids (Fig. 2), EPCAM signal was prominently detected and distributed throughout the spheroid, with nuclear DAPI staining confirming dense cellular organization, while decorin signal was minimal, consistent with the epithelial origin of this model. In contrast, CCD-112 mono-culture spheroids (Fig. 2) exhibited strong decorin expression with nuclear counterstaining, and little to no EPCAM signal, reflecting a stromal-like phenotype.

Following morphological and phenotypic validation of the spheroid models, the effects of PQ on metabolic activity were evaluated in CCD-112 fibroblast and Caco-2 tumor spheroids (Fig. 3). RLU values were normalized to the corresponding time matched DMSO controls to account for differences in baseline signal between the two models. In CCD-112 spheroids, fold changes generally remained below 1 across the evaluated concentrations and time points, indicating modest reductions in metabolic activity relative to vehicle. In contrast, Caco-2 spheroids generally exhibited fold changes above 1 during the intermediate time points. At 42 hours, CCD-112 spheroids remained below the vehicle reference across the available concentrations. The Caco-2 endpoint response was concentration dependent, ranging from below the vehicle control at 100 nM to near the vehicle response at 500 nM and above the vehicle response at 200 µM.

Following evaluation of PQ alone, Doxorubicin responses were assessed in Caco-2/CCD-112 co-culture spheroids in the absence or presence of PQ (Fig. 4). Doxorubicin alone produced concentration and time dependent reductions in metabolic activity relative to the corresponding DMSO controls (Fig. 4A). Higher concentrations produced earlier and larger reductions, whereas lower concentrations showed smaller or delayed responses. At 500 nM, the mean fold change decreased to approximately 0.29 at 24 hours and approached zero at 36 and 42 hours. Doxorubicin combined with PQ also produced concentration and time dependent changes in metabolic activity (Fig. 4B). At 500 nM, the combination initially produced mean fold changes of approximately 1.20 and 1.25 at 1 and 12 hours, respectively. This was followed by decreases to approximately 0.35 at 24 hours and 0.03 at both 36 and 42 hours. A direct comparison at 50 nM showed distinct response (Fig. 4C). Doxorubicin alone fluctuated around or above the DMSO reference throughout most of the experiment. In contrast, Doxorubicin combined with PQ initially increased above the DMSO reference before progressively decreasing after approximately 24 hours, reaching nearly zero by 42 hours. Overall, the largest reductions in metabolic activity occurred between 24 and 42 hours, with response patterns varying according to Doxorubicin concentration and PQ exposure.

Time effects of PQ on antineoplastic drug response were evaluated by calculating ΔAUC for Caco-2 monoculture and Caco-2/CCD-112 co-culture spheroids (Fig. 5). Doxorubicin produced mixed ΔAUC values across concentrations in both models. In Caco-2 monocultures, ΔAUC ranged from − 3.7 to 7.1, whereas co-culture values ranged from − 7.8 to 10.6. At 50 nM Doxorubicin, ΔAUC shifted from 4.3 in monoculture spheroids to − 7.8 in co-culture spheroids, indicating lower time integrated metabolic activity with PQ specifically in the co culture condition. Erlotinib exhibited a distinct culture dependent pattern. Caco-2 monocultures showed negative ΔAUC values from 10 to 100 nM, while co-cultures showed positive values over the same concentration range. Cediranib demonstrated the strongest concentration and context dependent pattern. Caco-2 monocultures showed negative ΔAUC values across all evaluated concentrations, with the largest reduction observed at 50 nM (− 30.0). In contrast, co-culture spheroids showed positive ΔAUC values from 10 to 100 nM, followed by negative values from 500 nM to 10 µM. Collectively, these results demonstrate that the magnitude and direction of PQ associated changes in metabolic activity varied according to drug, concentration, and spheroid composition.

Drug and drug interactions between PQ and Doxorubicin or Erlotinib were quantified using the Zero Interaction Potency (ZIP) model across full dose–response matrices (Fig. 6). ZIP δ-scores were calculated for each concentration pair to assess deviations from expected additive effects. In Caco-2 mono-culture spheroids, PQ and Doxorubicin combinations generated predominantly positive ZIP δ-scores across portions of the dose matrix, indicating localized regions of synergistic interaction. These regions were primarily observed at intermediate to higher concentration combinations, while lower concentration pairs showed ZIP δ-scores closer to zero, consistent with additive effects. The 2D synergy map demonstrated a gradient of increasing ZIP δ-scores across the matrix, which was further reflected in the 3D synergy landscape. The overall ZIP synergy score for this condition was 5.36, with a most synergistic area score of 20.18. In Caco-2 CCD-112 co-culture spheroids, PQ and Doxorubicin combinations produced a broader distribution of positive ZIP δ-scores across the dose matrix (Fig. 6). Compared to monoculture spheroids, larger regions of the matrix exhibited elevated ZIP δ-scores, particularly at higher concentration combinations of both agents. The 2D synergy map displayed expanded regions corresponding to positive δ-scores, and the 3D synergy surface showed increased peak values relative to mono-culture conditions. Lower concentration combinations remained closer to zero, indicating additive interactions in those regions.

The overall ZIP synergy score in co-culture spheroids was 12.71, with a most synergistic area score of 21.58. In contrast, PQ and Erlotinib combinations evaluated in Caco-2–CCD-112 co-culture spheroids produced ZIP δ-scores that were predominantly near zero or negative across the dose matrix (Fig. 6). The 2D synergy map showed limited regions of positive δ-scores, with most areas displaying neutral or negative values. The corresponding 3D synergy landscape exhibited a relatively flat profile with localized depressions corresponding to negative δ-scores. Higher concentration combinations did not produce consistent increases in ZIP δ-scores, and negative values were observed across multiple regions of the matrix. The overall ZIP synergy score for PQ and Erlotinib was − 0.74, with a most synergistic area score of 4.28. Across all evaluated conditions, ZIP δ-scores varied across concentration combinations, with regions of positive, neutral, and negative values observed within each dose response matrix. Two-dimensional heatmaps and three-dimensional landscapes consistently demonstrated non-uniform distributions of interaction effects across concentration pairs, with localized regions of elevated or reduced ZIP δ-scores corresponding to specific combinations of PQ and each agent.

Discussion

This study evaluated whether PQ alters antineoplastic drug response in 3D colorectal cancer spheroid models incorporating both mono-culture and epithelial with fibroblast co-culture systems. Our previous work showed that Cx43 overexpression in SW480 colorectal cancer cells produced an approximately sixfold increase in gap junction activity, while treatment with 200 nM PQ1 produced an approximately fourfold increase.[61] PQ1 also shifted Cx43 from the P0 isoform toward the more highly phosphorylated P2 isoform within one hour, suggesting that PQ1 may affect Cx43 processing or channel assembly in addition to total connexin abundance. This study provides direct support for the mechanistic premise of

the current work; however, it also highlights an important distinction.[21,61] Our previous work measured functional GJIC in a 2D colorectal cancer model, whereas the present study confirmed connexin expression but did not directly measure channel activity in the spheroids. Connexin expression does not necessarily indicate that the proteins are correctly localized at cell cell borders or assembled into functional channels. The limited and variable effect of PQ alone in the present study therefore does not necessarily contradict the previously reported increase in GJIC. Instead, it may indicate that PQ activity is influenced by the spatial organization, differentiation state, cell density, and accessibility of cell cell junctions within 3D spheroids. Our other previous work also found that PQ1 enhanced the antitumor activity of cisplatin in a T47D breast cancer xenograft model, accompanied by increased Cx43 and Cx26 expression and greater staining for apoptotic markers.[58] Although that study involved a different tumor type and antineoplastic agent, it supports the possibility that increasing connexin associated communication can amplify treatment induced stress or death signaling. The lack of uniform synergy in the present study suggests that this effect cannot be generalized across every drug or concentration. Doxorubicin induce DNA damage, but the intracellular signals generated and their effects on connexin phosphorylation or channel function may differ.

The concentration and model dependent patterns observed in the ΔAUC analysis further demonstrate that PQ did not produce a uniform change in drug response. When ΔAUC was defined as the AUC of the PQ drug combination minus the AUC of the corresponding drug alone, negative values indicated that PQ reduced cumulative metabolic activity, whereas positive values indicated that the combination maintained greater activity than the drug alone. Doxorubicin produced the most variable pattern. In coculture spheroids, the negative ΔAUC at 50 nM was consistent with late reduction in RLU, whereas positive values at 500 nM and 1 μM indicated that this enhancement was not maintained across higher concentrations. Erlotinib showed a clearer difference between models: PQ was associated with negative ΔAUC values in Caco-2 monocultures at 10–100 nM but positive values in co-culture spheroids over the same concentration range. This directional reversal suggests that fibroblast inclusion reduced or reversed the PQ associated enhancement of the erlotinib response at lower concentrations. Cediranib produced the clearest concentration by model interaction. Caco-2 monocultures showed negative ΔAUC values across the evaluated range, with the largest reductions at approximately 10–100 nM. By contrast, co-culture spheroids showed positive values at 10–100 nM and shifted toward negative values at 500 nM–10 μM. Thus, fibroblast inclusion appeared to increase the concentration threshold at which PQ was associated with a reduction in cumulative metabolic activity. These findings are consistent with Zoetemelk et al., who compared colorectal cancer cells in 2D cultures, tumor only spheroids, and heterotypic spheroids containing fibroblasts and endothelial cells.[62] They found that erlotinib sensitivity differed between 2D and 3D systems and that drug interactions could shift from synergistic or additive at lower concentrations to additive or antagonistic at higher concentrations. Stromal cell inclusion also increased resistance to selected combinations in some colorectal cancer cell lines but not others, demonstrating that the effect depended on both the cellular background and model composition. Valente et al. similarly found that fibroblast inclusion altered colorectal spheroid growth, viability, hypoxia, inflammatory signaling, extracellular-vesicle production, doxorubicin internalization, and

chemotherapy response.[63] In the present models, CCD-112 fibroblasts could influence drug responses by changing spheroid compactness and drug penetration, secreting survival factors, depositing extracellular matrix, or communicating directly with Caco-2 cells. Furthermore, because the assay measured the combined metabolic activity of both cellular populations, a lower co-culture RLU could reflect cancer cell death, fibroblast death, reduced proliferation or metabolism in either population, or a change in their relative abundance.

The ZIP results complement the time integrated ΔAUC analysis but address a different aspect of the response. The overall ZIP score of approximately 5.36 for PQ plus doxorubicin in Caco-2 monocultures falls within the conventionally additive range, despite the presence of a localized region with a higher score of approximately 20.18. In the co-culture model, the overall ZIP score increased to approximately 12.71, supporting overall synergy, with a most-synergistic region of approximately 21.58. In contrast, the overall ZIP score of approximately − 0.74 for PQ plus erlotinib indicates an additive interaction rather than overall antagonism, and its most synergistic region was only approximately 4.28. Therefore, the positive and negative δ-scores within the matrices should be described as localized interaction regions and should not be used to characterize the entire combination as synergistic or antagonistic. The higher doxorubicin ZIP score in co-culture, together with the negative ΔAUC observed at 50 nM, suggests that selected PQ doxorubicin concentrations may benefit from the presence of fibroblasts; however, the positive ΔAUC values at other doxorubicin concentrations show that this effect is not universal. Likewise, the mixed erlotinib and cediranib ΔAUC patterns demonstrate that interaction direction depends on both concentration and model composition. Collectively, the present results support a model in which PQ modifies antineoplastic drug responses in a concentration, drug, time, and microenvironment dependent manner rather than functioning as a universally synergistic agent.

Conclusions

This study demonstrates that PQ alters antineoplastic drug response in 3D colorectal cancer spheroid models, depending on drug type, concentration, and cellular context. PQ alone produced limited and variable effects on metabolic activity, whereas combination treatment with Doxorubicin resulted in greater reductions in RLU, particularly at later time points. ZIP analysis showed that drug interactions were non-linear across dose matrices and differed between mono-culture and co-culture systems. These findings support the use of 3D co-culture models and full dose response analyses to evaluate drug interactions and highlight that PQ effects are context dependent rather than uniformly synergistic.

Abbreviations

CRC
Colorectal cancer
3D
Three-dimensional
2D

Two-dimensional
PQ
Quinolone based gap junction enhancer
GJIC
Gap junction intercellular communication
Cx
Connexin
EPCAM
Epithelial cell adhesion molecule
DCN
Decorin
DAPI
4',6-diamidino-2-phenylindole
RLU
Relative luminescence units
ZIP
Zero Interaction Potency
DMSO
Dimethyl sulfoxide
SEM
Standard error of the mean
ATCC
American Type Culture Collection
PBS
Phosphate-buffered saline
FBS
Fetal bovine serum
RPMI
Roswell Park Memorial Institute medium

Declarations

Availability of data and materials

The datasets generated and analyzed during this study are included in this published article and its Supplementary Materials. This includes full dose response matrices, ZIP interaction outputs, and extended time course analyses.

Availability of data and materials

All data generated or analyzed during this study are included in this article and its Supplementary Materials.

Competing interests

The authors declare that they have no competing interests.

Funding
This work was supported by the Harrington Cancer and Health Foundation, Amarillo, TX, and Texas Tech University School of Veterinary Medicine, Amarillo, TX.

Acknowledgements

The authors thank the Texas Tech University School of Veterinary Medicine for institutional support.

Authors' contributions

Conceptualization – TL, TAN

Data curation – TL, TAN

Formal analysis– TL, TAN

Funding acquisition–TAN

Investigation– TL, TAN

Methodology– TL, TAN

Project administration– TAN

Resources–TAN

Software– TAN

Supervision–TAN

Validation– TL, TAN

Visualization– TL, TAN

Writing original draft – TL, TAN

Writing review and editing – TL, TAN

Authors’ information

Tomas Lugo and Thu Annelise Nguyen are affiliated with the School of Veterinary Medicine, Texas Tech University, Amarillo, TX, USA.

References

1. Lawler M, Johnston B, Van Schaeybroeck S, Salto-Tellez M, Wilson R, Dunlop M et al. Colorectal Cancer Abeloff's Clin Oncology 2019;: 1219–e128015.
2. Vogelstein B, Fearon ER, Hamilton SR, Kern SE, Preisinger AC, Leppert M, et al. Genetic Alterations during Colorectal-Tumor Development. N Engl J Med. 1988;319:525–32.
3. Elsaleh H, Grieu F, Joseph DJ, Iacopetta B. Molecular epidemiology of colorectal cancer. Int J Radiation Oncology*Biology*Physics. 2001;51. 10.1016/s0360-3016(01)02301-x.
4. Junttila MR, De Sauvage FJ. Influence of tumour micro-environment heterogeneity on therapeutic response. Nature. 2013;501. 10.1038/nature12626.
5. Wrzesinski K, Fey SJ. Metabolic reprogramming and the recovery of physiological functionality in 3D cultures in micro-bioreactors. Bioengineering. 2018;5. 10.3390/bioengineering5010022.
6. Loewenstein WR. Junctional intercellular communication: the cell-to-cell membrane channel. Physiol Rev. 1981;61:829–913.
7. Goodenough DA, Goliger JA, Paul DL. Connexins, connexons, and intercellular communication. Annu Rev Biochem. 1996;65:475–502.
8. De Wit C, Hoepfl B, Wölfle SE. Endothelial mediators and communication through vascular gap junctions. Biol Chem. 2006;387:3–9.
9. Yamada KM, Sixt M. Mechanisms of 3D cell migration. Nat Rev Mol Cell Biol. 2019;20. 10.1038/s41580-019-0172-9.
10. Mateos-Sánchez C, González B, de Miguel-García G, Font-Cugat A, Marcote-Corral I, Alonso S. Comparative analysis of 3D-culture techniques for multicellular colorectal tumour spheroids and development of a novel SW48 3D-model. Sci Rep. 2025;15. 10.1038/s41598-025-13588-x.
11. Cacciamali A, Villa R, Dotti S. 3D Cell Cultures: Evolution of an Ancient Tool for New Applications. Front Physiol. 2022;13. 10.3389/fphys.2022.836480.
12. Su CY, Burchett A, Dunworth M, Choi JS, Ewald AJ, Ahn EH, et al. Engineering a 3D collective cancer invasion model with control over collagen fiber alignment. Biomaterials. 2021;275. 10.1016/j.biomaterials.2021.120922.
13. Motta LCB, Pereira VM, Pinto PAF, Mançanares CAF, Pieri NCG, de Oliveira VC, et al. 3D culture of mesenchymal stem cells from the yolk sac to generate intestinal organoid. Theriogenology. 2023;209:98–106.
14. Lee HK, Noh MH, Hong SW, Kim SM, Kim SH, Kim YS, et al. Erlotinib Activates Different Cell Death Pathways in EGFR-mutant Lung Cancer Cells Grown in 3D Versus 2D Culture Systems. Anticancer Res. 2021;41:1261–9.

15. Liu R, Meng X, Yu X, Wang G, Dong Z, Zhou Z, et al. From 2D to 3D Co-Culture Systems: A Review of Co-Culture Models to Study the Neural Cells Interaction. Int J Mol Sci. 2022;23. 10.3390/ijms232113116.
16. Abbas ZN, Al-Saffar AZ, Jasim SM, Sulaiman GM. Comparative analysis between 2D and 3D colorectal cancer culture models for insights into cellular morphological and transcriptomic variations. *Scientific Reports 2023 13:1* 2023; 13: 1–16.
17. Jensen C, Teng Y. Is It Time to Start Transitioning From 2D to 3D Cell Culture? Front. Mol Biosci. 2020;7. 10.3389/fmolb.2020.00033.
18. De Maio A, Vega VL, Contreras JE. Gap junctions, homeostasis, and injury. J Cell Physiol. 2002;191:269–82.
19. Okamoto T, Suzuki K. The Role of Gap Junction-Mediated Endothelial Cell–Cell Interaction in the Crosstalk between Inflammation and Blood Coagulation. Int J Mol Sci. 2017;18:2254.
20. Nguyen SMT, Rupprecht CP, Haque A, Pattanaik D, Yusin J, Krishnaswamy G. Mechanisms governing anaphylaxis: Inflammatory cells, mediators, endothelial gap junctions and beyond. Int J Mol Sci. 2021;22. 10.3390/ijms22157785.
21. Bonacquisti EE, Nguyen J. Connexin 43 (Cx43) in cancer: Implications for therapeutic approaches via gap junctions. Cancer Lett. 2019;442:439–44.
22. Bigelow K, Nguyen TA. Increase of gap junction activities in SW480 human colorectal cancer cells. BMC Cancer. 2014;14:1–9.
23. Ding Y, Nguyen TA. Gap junction enhancer potentiates cytotoxicity of cisplatin in breast cancer cells. J Cancer Sci Ther. 2012;4. 10.4172/1948-5956.1000170.
24. Gong K, Hong Q, Wu H, Wang F, Zhong L, Shen L, et al. Gap junctions mediate glucose transfer to promote colon cancer growth in three-dimensional spheroid culture. Cancer Lett. 2022;531. 10.1016/j.canlet.2022.01.023.
25. Lee SW, Tomasetto C, Paul D, Keyomarsi K, Sager R. Transcriptional downregulation of gap-junction proteins blocks junctional communication in human mammary tumor cell lines. J Cell Biol. 1992;118:1213–22.
26. Livny O, Kaplan I, Reifen R, Polak-Charcon S, Madar Z, Schwartz B. Lycopene inhibits proliferation and enhances gap-junction communication of KB-1 human oral tumor cells. J Nutr. 2002;132. 10.1093/jn/132.12.3754.
27. Cottin S, Ghani K, de Campos-Lima PO, Caruso M. Gemcitabine intercellular diffusion mediated by gap junctions: New implications for cancer therapy. Mol Cancer. 2010;9. 10.1186/1476-4598-9-141.
28. Giepmans BNG. Gap junctions and connexin-interacting proteins. Cardiovasc Res. 2004;62:233–45.
29. Rossetti M, Stanca S, Del Frate R, Bartoli F, Marciano A, Esposito E, et al. Tumor Progression from a Fibroblast Activation Protein Perspective: Novel Diagnostic and Therapeutic Scenarios for Colorectal Cancer. Diagnostics (Basel). 2023;13. 10.3390/diagnostics13203199.

30. Liu J, Zhang Y. Intratumor microbiome in cancer progression: current developments, challenges and future trends. Biomark Res. 2022;10. 10.1186/s40364-022-00381-5.
31. Marushima H, Shibata SI, Asakura T, Matsuura T, Maehashi H, Ishii Y, et al. Three-dimensional culture promotes reconstitution of the tumor-specific hypoxic microenvironment under TGFβ stimulation. Int J Oncol. 2011;39. 10.3892/ijo.2011.1142.
32. Bejarano L, Jordão MJC, Joyce JA. Therapeutic targeting of the tumor microenvironment. Cancer Discov. 2021;11:933–59.
33. Yang Y, Weng W, Peng J, Hong L, Yang L, Toiyama Y, et al. Fusobacterium nucleatum Increases Proliferation of Colorectal Cancer Cells and Tumor Development in Mice by Activating Toll-Like Receptor 4 Signaling to Nuclear Factor – κB, and Up-regulating Expression of MicroRNA-21. Gastroenterology. 2017;152. 10.1053/j.gastro.2016.11.018.
34. de Visser KE, Joyce JA. The evolving tumor microenvironment: From cancer initiation to metastatic outgrowth. Cancer Cell. 2023;41. 10.1016/j.ccell.2023.02.016.
35. Binnewies M, Roberts EW, Kersten K, Chan V, Fearon DF, Merad M, et al. Understanding the tumor immune microenvironment (TIME) for effective therapy. Nat Med. 2018;24. 10.1038/s41591-018-0014-x.
36. Kang J, La Manna F, Bonollo F, Sampson N, Alberts IL, Mingels C, et al. Tumor microenvironment mechanisms and bone metastatic disease progression of prostate cancer. Cancer Lett. 2022;530. 10.1016/j.canlet.2022.01.015.
37. Brennen WN, Isaacs JT, Denmeade SR. Rationale behind targeting fibroblast activation protein-expressing carcinoma-associated fibroblasts as a novel chemotherapeutic strategy. Mol Cancer Ther. 2012;11:257–66.
38. Schiff PB, Horwitz SB. Taxol stabilizes microtubules in mouse fibroblast cells. Proc Natl Acad Sci U S A. 1980;77:1561.
39. Li S, Lu R, Shu L, Chen Y, Zhao J, Dai J, et al. An integrated map of fibroblastic populations in human colon mucosa and cancer tissues. Commun Biol. 2022;5. 10.1038/s42003-022-04298-5.
40. Yang D, Liu J, Qian H, Zhuang Q. Cancer-associated fibroblasts: from basic science to anticancer therapy. Exp Mol Med. 2023;55. 10.1038/s12276-023-01013-0.
41. Yoshida GJ. Regulation of heterogeneous cancer-associated fibroblasts: The molecular pathology of activated signaling pathways. J Experimental Clin Cancer Res. 2020;39. 10.1186/s13046-020-01611-0.
42. La Vecchia S, Sebastián C. Metabolic pathways regulating colorectal cancer initiation and progression. Semin Cell Dev Biol. 2020;98. 10.1016/j.semcdb.2019.05.018.
43. Kim J, Lee HK. Potential Role of the Gut Microbiome In Colorectal Cancer Progression. Front Immunol. 2022;12. 10.3389/fimmu.2021.807648.
44. Kim SH, Park DH, Lim YJ. Impact of Diet on Colorectal Cancer Progression and Prevention: From Nutrients to Neoplasms. Korean J Gastroenterol. 2023;82. 10.4166/kjg.2023.079.

45. Their JP. Epithelial-mesenchymal transitions in tumour progression. Nat Rev Cancer. 2002;2:442–54.
46. Bajaj J, Diaz E, Reya T. Stem cells in cancer initiation and progression. J Cell Biol. 2020;219. 10.1083/jcb.201911053.
47. Sheth M, Esfandiari L. Bioelectric Dysregulation in Cancer Initiation, Promotion, and Progression. Front Oncol. 2022;12. 10.3389/fonc.2022.846917.
48. Klein CA. Cancer progression and the invisible phase of metastatic colonization. Nat Rev Cancer. 2020;20. 10.1038/s41568-020-00300-6.
49. Derynck R, Akhurst RJ, Balmain A. TGF-β signaling in tumor suppression and cancer progression. Nat Genet. 2001;29. 10.1038/ng1001-117.
50. Zhou M, Zheng M, Zhou X, Tian S, Yang X, Ning Y, et al. The roles of connexins and gap junctions in the progression of cancer. Cell Communication Signal. 2023;21. 10.1186/s12964-022-01009-9.
51. Gonzalez H, Hagerling C, Werb Z. Roles of the immune system in cancer: From tumor initiation to metastatic progression. Genes Dev. 2018;32. 10.1101/GAD.314617.118.
52. Kapałczyńska M, Kolenda T, Przybyła W, Zajączkowska M, Teresiak A, Filas V, et al. 2D and 3D cell cultures – a comparison of different types of cancer cell cultures. Archives Med Sci. 2018;14. 10.5114/aoms.2016.63743.
53. Lederer S, Dijkstra TMH, Heskes T. Additive dose response models: Defining synergy. Front Pharmacol. 2019;10. 10.3389/fphar.2019.01384.
54. Goutelle S, Maurin M, Rougier F, Barbaut X, Bourguignon L, Ducher M, et al. The Hill equation: A review of its capabilities in pharmacological modelling. Fundam Clin Pharmacol. 2008;22. 10.1111/j.1472-8206.2008.00633.x.
55. Chen D, Liu X, Yang Y, Yang H, Lu P. Systematic synergy modeling: Understanding drug synergy from a systems biology perspective. BMC Syst Biol. 2015;9. 10.1186/s12918-015-0202-y.
56. Lederer S, Dijkstra TMH, Heskes T. Additive dose response models: Explicit formulation and the Loewe Additivity Consistency Condition. Front Pharmacol. 2018;9. 10.3389/fphar.2018.00031.
57. Yadav B, Wennerberg K, Aittokallio T, Tang J. Searching for Drug Synergy in Complex Dose-Response Landscapes Using an Interaction Potency Model. Comput Struct Biotechnol J. 2015;13. 10.1016/j.csbj.2015.09.001.
58. Shishido S, Nguyen TA. Combinational treatment of gap junction enhancers and paclitaxel attenuates mammary tumor growth. Anticancer Drugs. 2020;31:353–8.
59. Gakhar G, Schrempp D, Nguyen TA. Regulation of gap junctional intercellular communication by TCDD in HMEC and MCF-7 breast cancer cells. Toxicol Appl Pharmacol. 2009;235:171–81.
60. Gakhar G, Ohira T, Shi A, Hua DH, Nguyen TA. Antitumor effect of substituted quinolines in breast cancer cells. Drug Dev Res. 2008;69:526–34.
61. Bigelow K, Nguyen TA. Increase of gap junction activities in SW480 human colorectal cancer cells. BMC Cancer. 2014;14:1–9.

62. Zoetemelk M, Rausch M, Colin DJ, Dormond O, Nowak-Sliwinska P. Short-term 3D culture systems of various complexity for treatment optimization of colorectal carcinoma. Sci Rep. 2019;9. 10.1038/s41598-019-42836-0.
63. Valente R, Cordeiro S, Luz A, Melo MC, Rodrigues CR, Baptista PV, et al. Doxorubicin-sensitive and -resistant colorectal cancer spheroid models: assessing tumor microenvironment features for therapeutic modulation. Front Cell Dev Biol. 2023;11. 10.3389/fcell.2023.1310397.

Figures

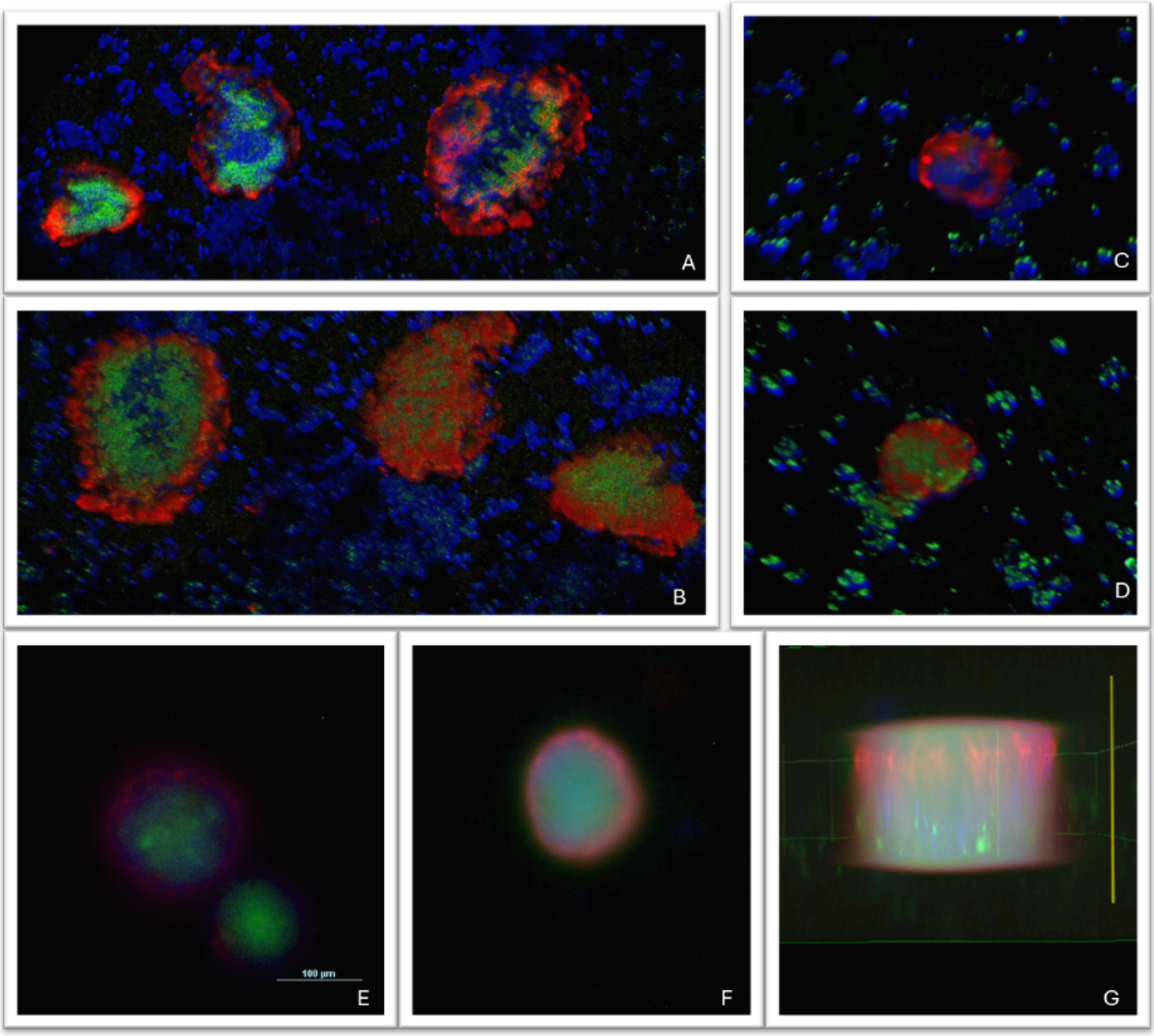


Figure 1

Confocal characterization of colorectal cancer cell line–CCD-112 co-culture spheroids. Representative confocal images showing DAPI-stained nuclei (blue), epithelial cell adhesion molecule (EPCAM)-positive colorectal cancer cells (red), and decorin positive CCD-112 fibroblasts (green). (A) Front-view and (B) back-view images of Caco-2–CCD-112 co-culture spheroids demonstrate consistent epithelial–stromal organization across opposing orientations. (C) Front-view and (D) back-view images of HT-29–CCD-112 co-culture spheroids show EPCAM-positive HT-29 cells forming compact epithelial regions, with decorin positive CCD-112 fibroblasts interspersed throughout the surrounding spheroid structure. (E–G) Z-stack confocal images of SW620–CCD-112 co-culture spheroids demonstrate maintenance of EPCAM-positive SW620 cells and decorin positive fibroblasts across multiple optical sections, confirming three-dimensional epithelial–stromal integration within the spheroid architecture.

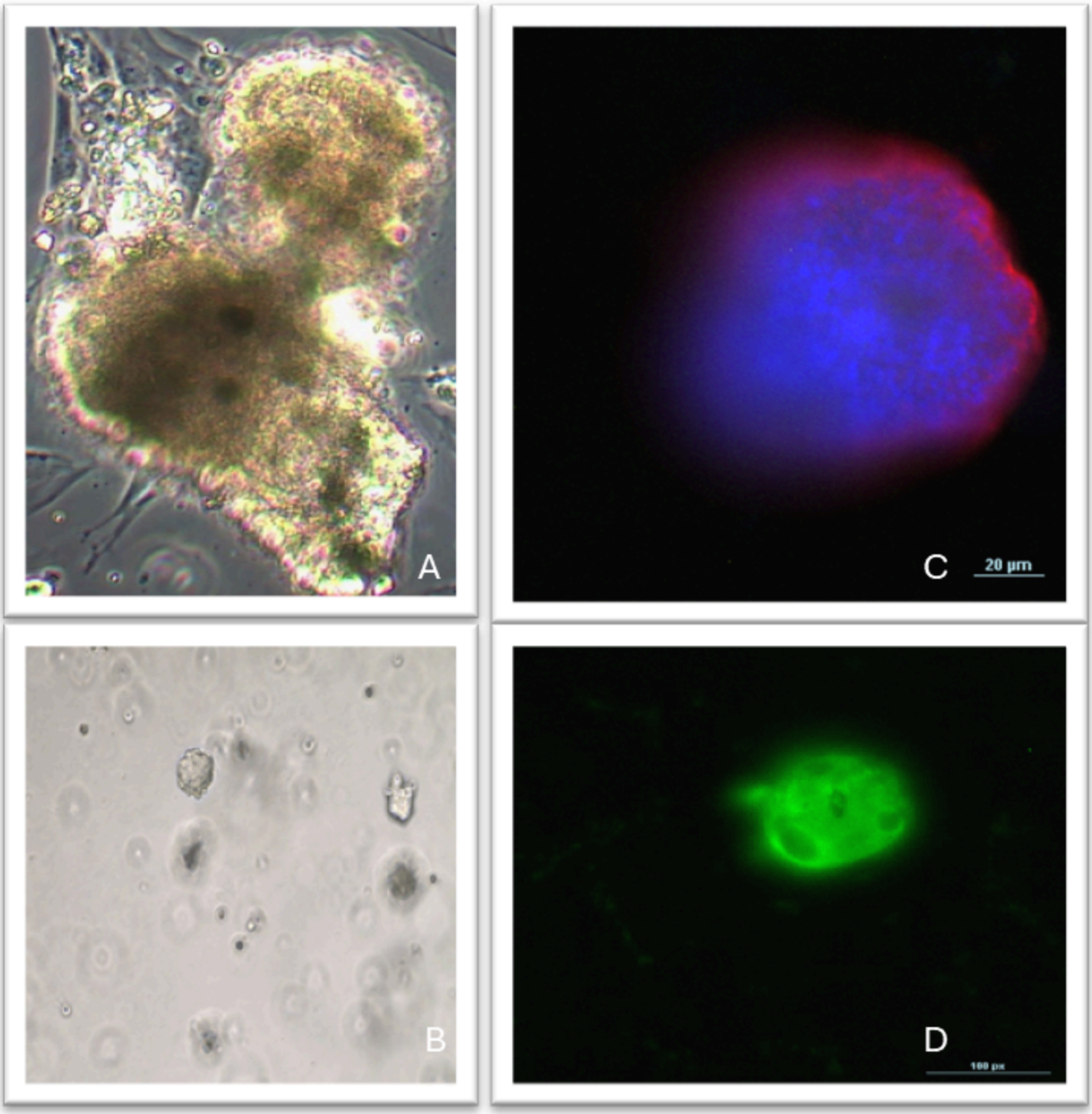


Figure 2

Morphological and marker characterization of monoculture and co-culture spheroids. Representative brightfield and confocal images comparing Caco-2 monoculture, CCD-112 monoculture, and Caco-2–CCD-112 co-culture spheroids. (A) Brightfield image of Caco-2–CCD-112 co-culture spheroids showing spheroid morphology under co-culture conditions. (B) Brightfield image of Caco-2 monoculture spheroids showing compact morphology in the absence of fibroblast co-culture. (C) Confocal image of Caco-2 monoculture spheroids showing EPCAM expression in Caco-2 cells (red), decorin signal (green),

and nuclear counterstaining with DAPI (blue). (D) Confocal image of CCD-112 monoculture spheroids showing decorin expression in fibroblasts (green), EPCAM signal (red), and DAPI-stained nuclei (blue).

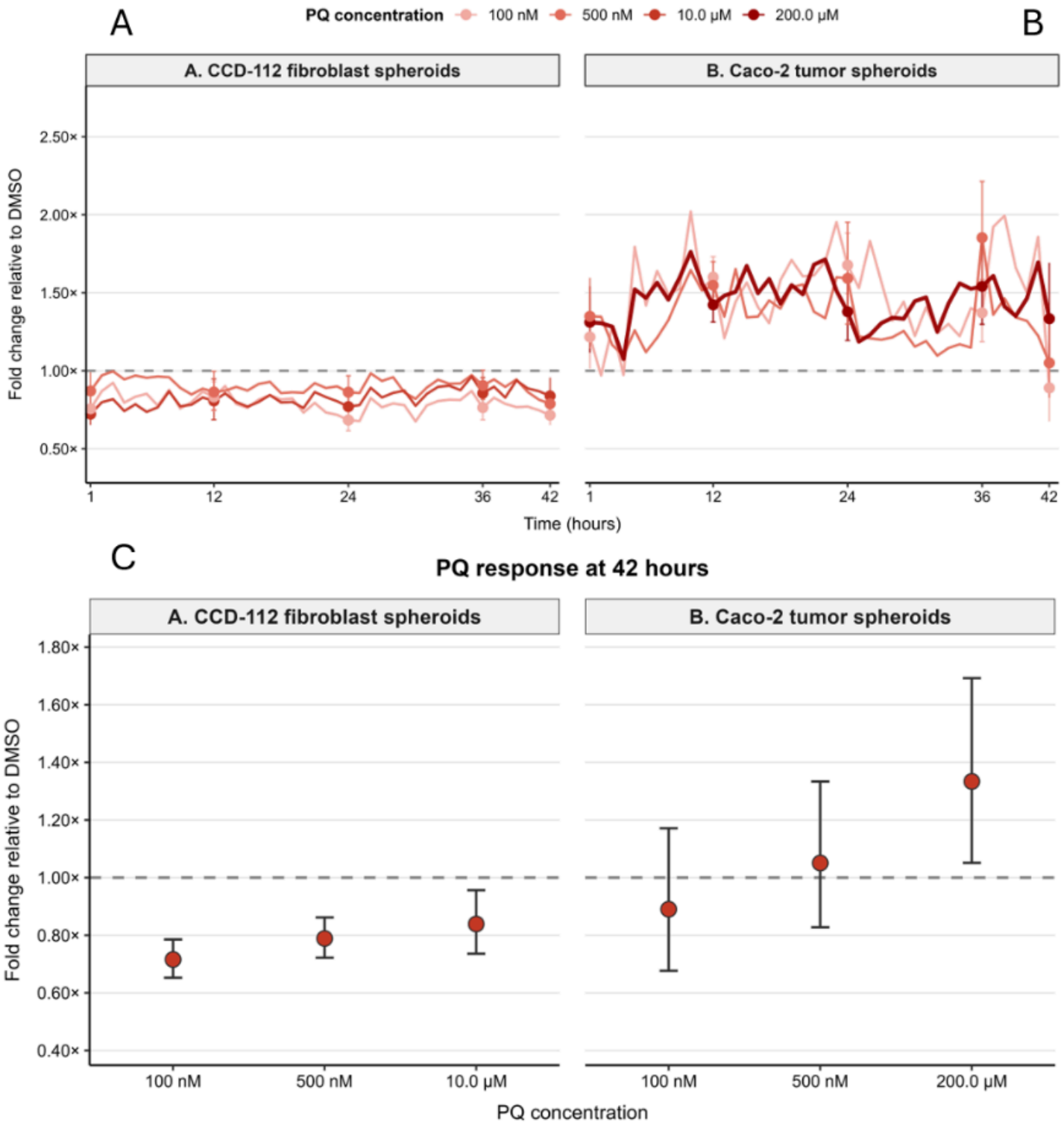


Figure 3

Concentration and time dependent effects of PQ on metabolic activity in fibroblast and colorectal cancer spheroids. CCD-112 fibroblast and Caco-2 colorectal cancer spheroids were treated with PQ

concentrations, and metabolic activity was monitored using RealTime-Glo luminescence. RLU values were normalized to the corresponding time matched DMSO controls and are presented as fold changes. (A) Time dependent PQ responses in CCD-112 fibroblast spheroids. (B) Time dependent PQ responses in Caco-2 tumor spheroids. Lines represent mean fold changes, and error bars represent SEM at selected time points. (C) PQ concentration response at 42 hours in each spheroid model. In all panels, the dashed line at 1 indicates no difference from the vehicle control; values below 1 indicate lower metabolic activity, whereas values above 1 indicate higher metabolic activity relative to DMSO.

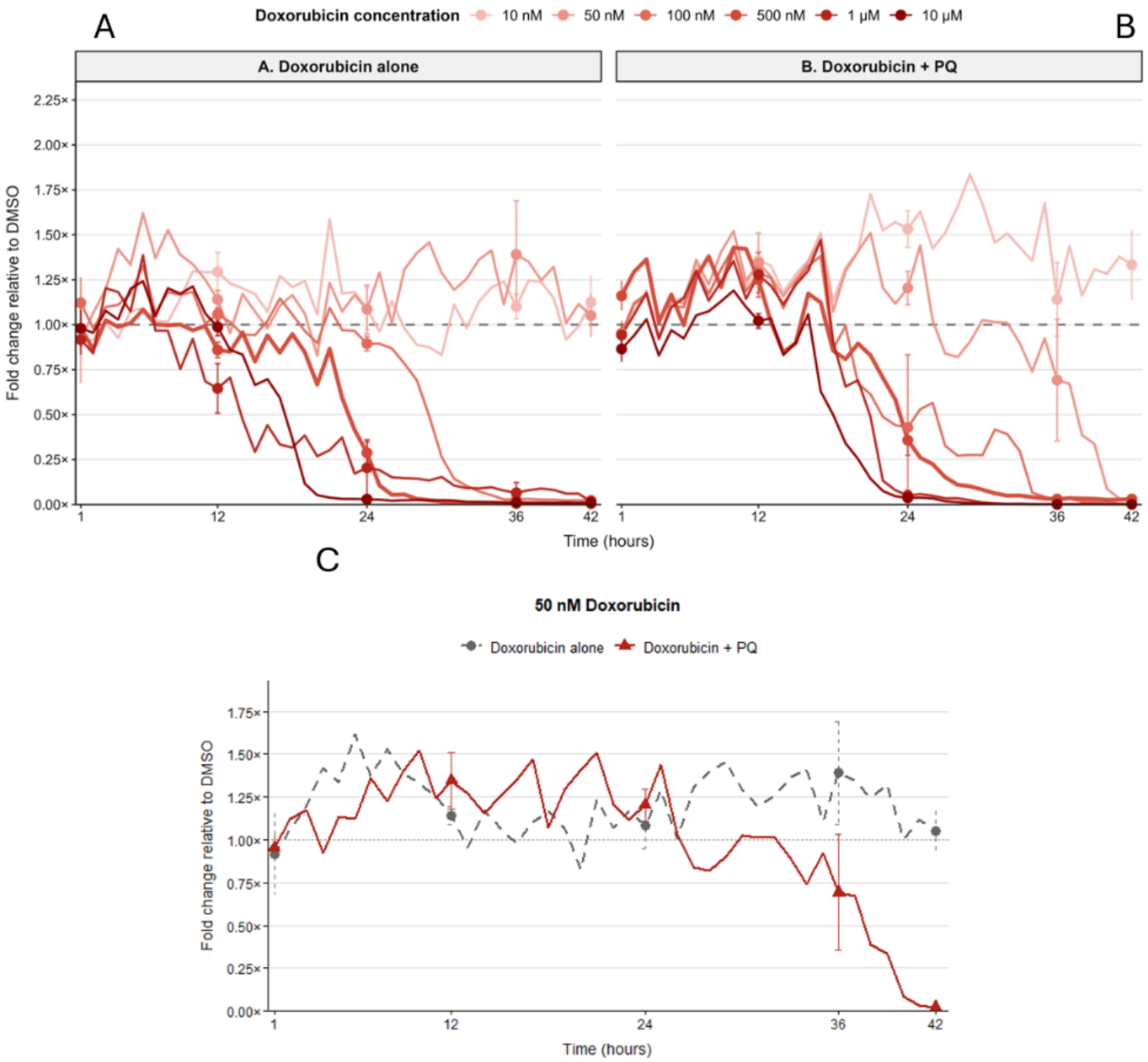


Figure 4

Concentration and time dependent Doxorubicin responses in Caco-2/CCD-112 co-culture spheroids with and without PQ. Co-culture spheroids were treated with the Doxorubicin concentrations in the absence (A) or presence (B) of PQ, and metabolic activity was monitored using RealTime-Glo luminescence. RLU values were normalized to the corresponding time matched DMSO controls and are presented as fold changes. Lines represent mean fold changes, and error bars represent SEM at selected time points. The dashed line at 1 indicates no difference from vehicle; values below 1 indicate reduced metabolic activity, whereas values above 1 indicate increased metabolic activity relative to DMSO. (C) Direct comparison of 50 nM Doxorubicin in the absence and presence of PQ.

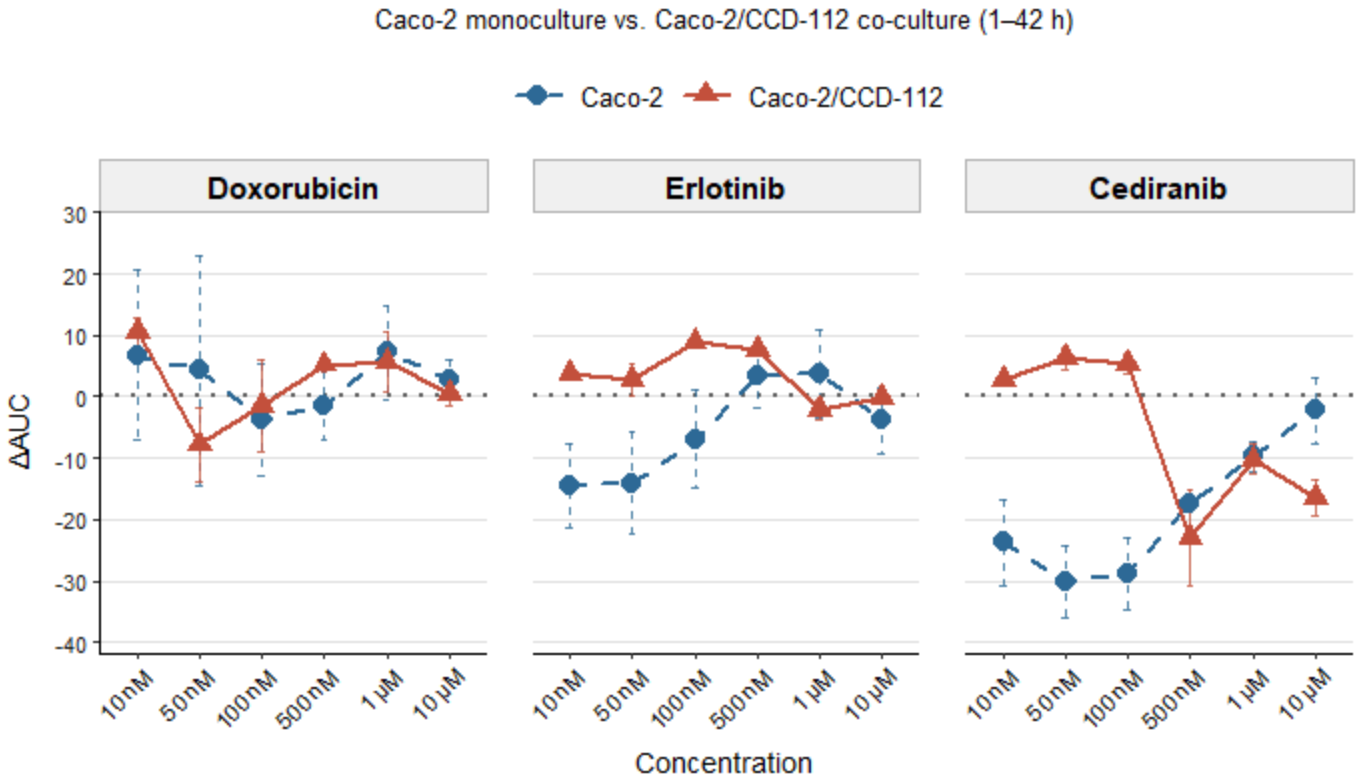


Figure 5

PQ changes in drug response in Caco-2 monoculture and Caco-2/CCD-112 co-culture spheroids. *Metabolic activity was monitored from 1 to 42 hours following treatment with Doxorubicin, Erlotinib, or Cediranib in the absence or presence of PQ. RFU values were normalized to the corresponding DMSO controls, and AUC was calculated for each replicate. ΔAUC was defined as* $AUC_{drug + PQ} - AUC_{Alone}$. *Negative values indicate lower metabolic activity with PQ, whereas positive values indicate higher activity with PQ. Points represent mean ΔAUC from three replicates, error bars represent SEM, and lines connect concentrations The dotted line at zero indicates no difference between drug alone and drug plus PQ conditions.*

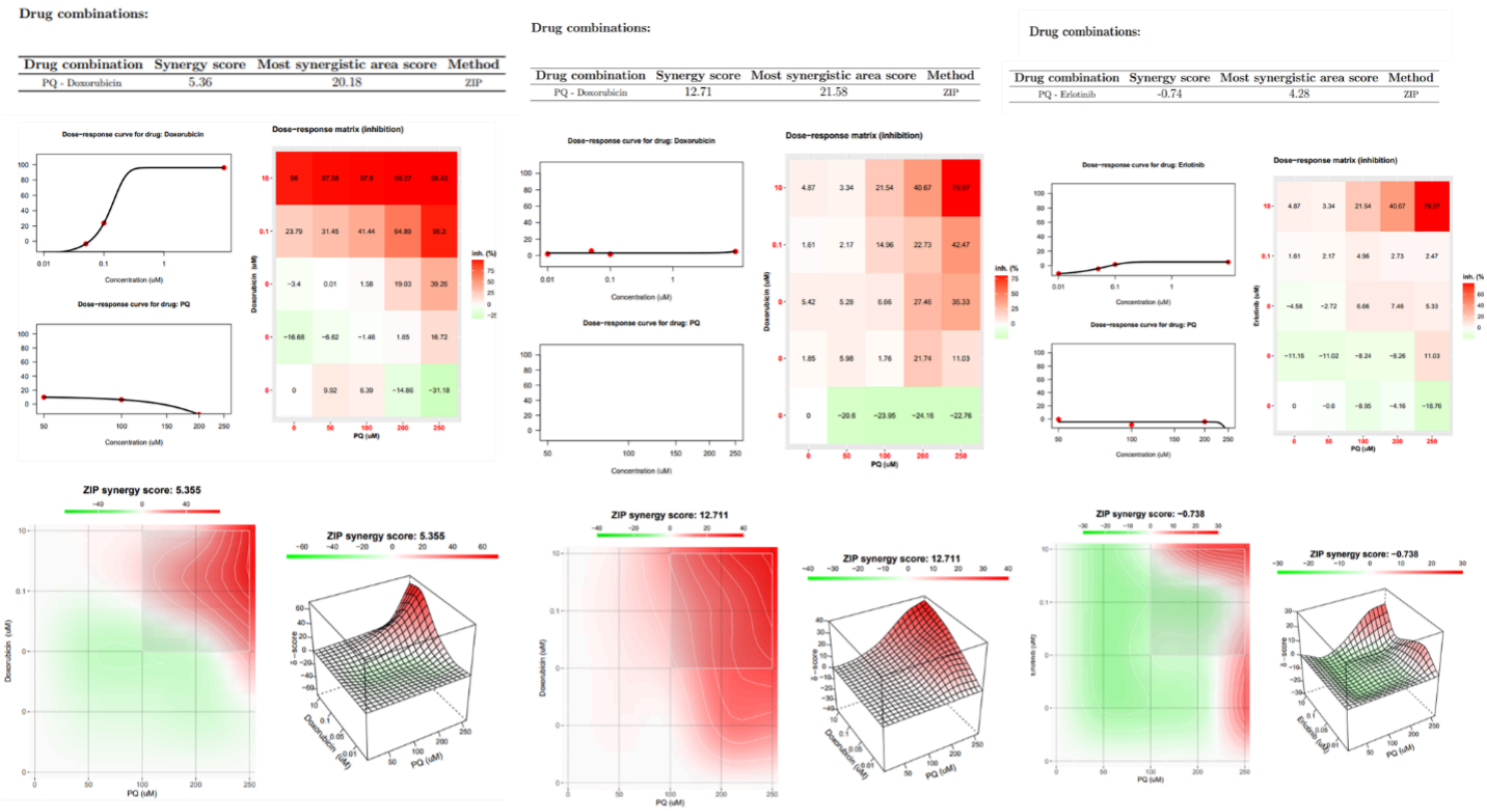


Figure 6

ZIP synergy analysis of PQ in combination with antineoplastic agents in colorectal cancer spheroids. Drug-drug interactions between PQ and Doxorubicin or Erlotinib were evaluated using the Zero Interaction Potency (ZIP) model in both Caco-2 mono-culture and Caco-2–CCD-112 co-culture spheroids. Dose response curves for individual agents and corresponding inhibition matrices summarize single-agent and combination effects across concentration ranges. Two-dimensional ZIP synergy maps and three-dimensional synergy landscapes display the distribution of ZIP δ-scores across each drug–dose matrix, with red regions indicating synergistic interactions and green regions indicating antagonism .In Caco-2 mono-culture spheroids, PQ and Doxorubicin exhibited modest synergy (ZIP score: 5.36; most synergistic area: 20.18). In co-culture spheroids, PQ and Doxorubicin demonstrated increased synergy (ZIP score: 12.71; most synergistic area: 21.58). In contrast, PQ and Erlotinib interactions in co-culture spheroids showed predominantly additive to weakly antagonistic effects (ZIP score: −0.74; most synergistic area: 4.28).